FURTHER SIMULATION OF THE PRESSURE TUBE CIRCUMFERENTIAL TEMPERATURE DISTRIBUTION EXPERIMENTS (MAKE-UP WATER SERIES)

M. Bayoumi, W.C. Muir, and P.S. Kundurpi

* Ontario Hydro, Nuclear Safety Department
700 University Avenue, Toronto, Ontario, M5G 1X6
** IDEA Research International

ABSTRACT

Under some postulated accident scenarios in a CANDU reactor, some fuel channels may experience periods of stratified flow in which the top portion of the pressure tube and fuel elements are exposed to superheated steam while the bottom portion is cooled with water. As a result, the upper part heats up and a temperature gradient is developed around the circumference of the pressure tube. This temperature gradient could result in a nonuniform or localized pressure tube strain which could lead to failure of the pressure tube prior to contacting the calandria tube. The pressure tube circumferential temperature experimental program (PT-DELTA T) has been ongoing at AECL-WNRE under COG to investigate the potential of pressure tube rupture during ballooning, prior to contacting the calandria tube, in pressure tubes exposed to stratified coolant conditions.

The main objective of this paper is to discuss the simulation results of three of the Make-Up Water experiments using the SMARTT (Simulation Method for Azimuthal and Radial Temperature Transients) [1] computer code and to compare with the experimental results for code verification. A discussion and analysis of the information gained from these experiments are presented.

INTRODUCTION

The experimental programme was designed to simulate different phases of feeder draining which range from the early stages to the most severe scenario. Three distinct phases of feeder draining have been identified [2], namely, boil-off, steady-steaming, and steam-cooling. In the boil-off stage, the channel and end-fittings experience a period of sustained liquid boil off in which the extent of fuel element overheating progressively increases. In the steady-steaming phase which corresponds to the early stages of feeder draining, the inlet feeder and inlet end-fitting are filled with liquid which is close to saturation whereas the outlet header is completely voided with no liquid to counter flow down the outlet feeder and, thus, reduce the established density driving head. In the steam-cooling phase, the liquid level

drops below the inlet feeder connection to the inlet header and is characterised by a steadily decreasing density driving head as the liquid level in the feeder decreases. In this phase, depending on the header conditions, decreasing flow rate of single or two phase flow from the inlet feeder into the channel is established.

Four experimental series have been completed at WNRE to cover the different stages of feeder draining. The Boil-off series was designed to examine situations when the coolant flow is stagnated [3,4] (channel Boil-Off phase). In the Make-up water series the coolant level is maintained constant by injecting make-up-water to balance the steam flow out of the channel to simulate the steady steaming phase (Make-Up-Water series) [5]. In the third series, Steam Cooling series, superheated steam and make-up water are injected simultaneously into one end of the pressure tube. This simulates a postulated LOCA situation in which the inlet header is partially voided, resulting in water and steam flow through the heated fuel channel. In the fourth test series, Variable Make-Up Water, water is injected into the pressure tube at a controlled and declining rate to study the effect of a gradual decrease in make-up water flow rate to simulate the decreasing density driving head as the liquid level in the feeder decreases. The third and fourth series of the experiments are designed to simulate different stages of feeder draining phase.

A BRIEF DESCRIPTION OF THE SMARTT CODE

The SMARTT computer code [1] is one of the analytical tools used in the analysis of fuel channel integrity in general. The code is used in the safety analysis of CANDU reactors to predict fuel and pressure tube thermal and mechanical behaviour under asymmetric coolant conditions such as stratified coolant flow. In the stratified flow regime, the top portion of the pressure tube and fuel elements are exposed to superheated steam while the bottom portion is cooled with saturated or slightly subcooled water. Such conditions can lead to non-uniform pressure tube heatup in the circumferential direction. If a highly localized hot spot develops on the pressure tube circumference while the pressure tube is undergoing transverse strain (ballooning), the pressure tube could rupture prior to contacting the

calandria tube. The code predicts the pressure tube circumferential temperature distribution and its effect on pressure tube ballooning. The code also predicts whether the pressure tube will rupture prior to contacting the calandria tube or balloon into contact with the calandria tube.

SMARTT is a two-dimensional heat transfer code which models half of the bundle cross-section at one axial position in a fuel channel assuming symmetry across the vertical plane. The 37-element bundle model includes a circumferentially and radially conducting pressure tube with 16 full fuel-element models, and five half-fuel element models. Figure 1 shows the azimuthal nodalization of a 37-element fuel bundle.

Each fuel element is divided into six radial nodes; four nodes for the fuel, one node for the gap and one node for the sheath. The fuel nodes are chosen to have equal area and therefore approximately equal power production. The full element models in SMARTT are divided into eight equal azimuthal nodes; the centre half element has six nodes; and the other half elements have four nodes. The pressure tube is divided into four radial nodes and 36 circumferential nodes, each subtending an angle of 5 degrees.

The code uses transient thermohydraulic conditions, either predicted by another code or calculated within. The flow area between the fuel elements and the pressure tube is divided into 30 subchannels for the 37-element (Figure 1) model. The coolant temperature is assumed uniform within each subchannel.

The required transient boundary conditions consist of:

- 1 The coolant temperature for each subchannel.
- 2 The sheath-to-coolant and coolant-to-pressure tube heat transfer coefficients for each fuel and pressure tube surface.
- 3 the fuel power transient.

The modes of heat transfer accounted for are:

- 1 Radial and azimuthal conduction within each fuel element.
- Convection from sheath-to-coolant and coolant-topressure tube.
- Radiation among all outer fuel sheath and inner pressure tube surface nodes.
- 4 Radial and circumferential conduction within the pressure tube.
- 5 Radiation and conduction across the gas gap between the pressure tube and the calandria tube.

The modes of heat production considered are:

- Fission and decay power with bundle and element flux depression.
- 2 Metal-water reaction on sheath outer surfaces and the inner surface of the pressure tube.
- 3 Internal gamma heating of the pressure tube (usually small).

The liquid level in SMARTT is modelled in seven discrete levels due to the nodalization of the channel flow area into subchannels. The liquid levels modelled are: 100%, 76%, 58%, 42%, 24%, 8% and 0% for the 37-element model. The percentages indicate the fraction of total channel flow area covered by the liquid. The falling liquid level is simulated by moving through the discrete levels, switching instantaneously from one to the next.

The transverse pressure tube strain calculation is based on the computer code NUBALL [6]. The transverse strain rate equations used in this code were experimentally verified. This approach provides both the average pressure tube strain as a function of time, and the local strain (wall thinning) at each circumferential node. Based on these information, it is possible to determine whether or not the pressure tube achieves sufficient average strain to contact the calandria tube (about 16% average diametral strain), before local wall thinning at the hot spot causes the pressure tube to rupture.

DESCRIPTION OF EXPERIMENTAL APPARATUS AND INSTRUMENTATION

The apparatus for these tests consisted of a network of inlet piping (Figure 2) which was connected to the make-up boiler at one end and to the inlet of the test section at the other. The inner diameter of the piping was 5 mm. Water was extracted from the boiler, passed through this network of piping and injected into the test section. A flow restrictor valve, located in front of the inlet of the test section, was used to adjust the water flow rate. A coiled heat exchanger was available to control the temperature of the "make-up" water [5].

The test section consisted of a 2.33 metre long, horizontal segment of a CANDU-type fuel channel with a water inlet pipe (5 mm ID) at the bottom of one end and an exit pipe (24.3 mm ID) at the top of the other end (Figure 3). The fuel-element simulators (Figure 4) for the 37-element bundle configuration were composed of a Zircaloy tube (concentric with the Zircaloy fuel-element sheath) which was heated electrically. The fuel elements were grouped electrically into three rings with no electrical connection to the central element. High-temperature thermocouples were placed around the outside of the pressure tube, at the top of the calandria tube, and on several of the fuel-element sheaths at three axial locations along the test section. A thermocouple

was also placed at the channel exit to measure the steam temperature. Linear voltage displacement transducers were placed on the calandria tube to record the absolute and relative motion of the calandria tube with respect to the pressure tube. The test section was immersed in a water bath to simulate the moderator.

EXPERIMENTAL PROCEDURE AND RESULTS

Initially, the test section was filled with water at room temperature and pressurized to the required pressure in each experiment. The water surrounding the calandria tube was then heated to the pre-specified experiment temperature to simulate the moderator. This was followed by a long start-up period during which the pressurized water in the test section was gradually raised to saturation.

In order to maintain a uniform temperature throughout the test section, six bottom heaters of the outer ring and six bottom heaters of the middle ring were connected to the power supply and a low power (depending on the experiment pressure) was used to heat up the water. This procedure reduced the top-to-bottom temperature gradient across the test section as the water temperature was slowly raised to saturation. With valve 1 closed and valve 2 open, the flow was set while the channel was pre-heated. Once the flow and channel temperature were stabilized, the flow was diverted into the test section by closing valve 2 and opening valve 1. The back pressure in the by-pass line was kept equal to that Flow through the channel was of the test section. maintained for half an hour to obtain steady state before the power was ramped up to the desired level for the test. The annulus between the pressure and calandria tubes was purged with CO₂. The purge flow was high initially but reduced to near stagnation just before the start of the test.

A pre-specified power history was applied to the test section and the experiment was terminated shortly after pressure tube ballooning into contact with the calandria tube or upon failure of the pressure tube.

EXPERIMENT 1

The channel pressure in this experiment was constant at 1.1 MPa. The transient power history is shown in Figure 5. The maximum power input to the heaters was about 40 kW. The make-up water flow rate was 8.2 g/s. The power was maintained approximately at 38.5 kW until 1111 s into the test. At this time some of the heaters failed. More heater failures occurred at 1153 s and 1212 s and the power dropped to 33 kW. The experiment was allowed to continue at this power level until 1545 s. At this time the power supply was switched off and the test was terminated. The differential transmitters connected to the orifice to measure

exit steam flow of the channel failed. Therefore, no data are available on exit steam flow rates for this test.

Post experiment examination of the test section showed that the top of the pressure tube had contacted with the calandria tube near the steam exit (100 mm from the steam exit, and axially approximately 300 mm towards Ring 1). Based on the nucleate boiling observation on the outside surface of the calandria tube, it was concluded that the pressure tube contacted the calandria tube at times between 1000 and 1100 s into the test.

The LVDT measurement at Ring 1 also indicated that the pressure tube did not contact the calandria tube at that location. The following argument could explain the decline in the pressure tube temperature at the top at Ring 1. As the top of the pressure tube heated up, it ballooned away from the heaters. This caused the flow to bypass from the inside of the inner subchannel into the larger area of the outer subchannel resulting in increased steam cooling at the top of the pressure tube. Also, as the gap between the pressure tube and calandria tube decreased, the conductive heat loss to the calandria tube became more efficient. These two effects combined with the axial conduction to the region of pressure/calandria tube contact contributed to the cooling of the pressure tube at Ring 1.

EXPERIMENT 2

Power input and make-up water flow rate were the major differences between experiments 2 and 1. The peak power input was 87 kW as opposed to 40 kW in experiment 1. The transient power history is shown in Figure 6. The make-up water flow rate was 26 g/s vs. 8.2 g/s in the first experiment.

The power increased gradually to a maximum of 80 kW at approximately 99 s. It decreased to 76 kW at 250 s at which time some heaters failed and the power dropped quickly to zero.

At time 245 s, the temperature at the top of the pressure tube started to decrease. At the same time, the calandria tube temperature rose more sharply. This simultaneous drop in pressure tube temperature and a corresponding rise in the calandria tube temperature, indicated that the pressure tube at Ring 3 ballooned into contact with the calandria tube. However, because the rate of the reduction in pressure tube temperature was small (4°C/s), it was concluded that the contact was not as hard as observed in the boil-off experiments. The top of the pressure tube reached a maximum temperature of 854°C at Ring 3 at time 245 s, 5 s prior to the heater failure. After the heater failure, at 259 s into the experiment, the pressure tube ruptured.

Post experiment examination of the test section revealed that the rupture/crack started at about 2 mm downstream of Ring 2 at the top near mid-plane. The total rupture length was 290 mm. The heaters were damaged at locations around both Rings 2 and 1 while the heaters around Ring 3 were intact. These observations indicate that the pressure tube rupture was caused by localized heating due to the heater failure.

EXPERIMENT 3

The objective of this experiment was to investigate the circumferential temperature distribution developed on a half-full and less than half-full pressure tube under constant channel pressure of 4 MPa and total heater power of 80 kW. The transient power history is shown in Figure 7. The make-up water flow rate in this experiment was 26 g/s.

The power history (Figure 7) can be divided into three periods: 0 - 529 s, 529 - 1070 s and 1070 - 1277 s. In the first period, power was ramped to just over 80 kW and stabilized at 83 kW by time 296 s. Towards the end of the first period, the pressure tube was slightly more than halffull of water. During the second period, power was ramped to 89.3 kW and the water level subsequently decreased approximately to mid-height. During the third period, power was further increased to 99 kW and the water level dropped to slightly less than half-full.

At time 1159 s in the second phase, heaters in the top part of the outer ring began to fail. At time 1278 s during the third phase, the pressure tube ruptured. After the pressure tube failure, the calandria tube also ruptured.

During the first period, the top of the pressure tube reached a maximum temperature of approximately 700°C. In the second period, when the power increased, the pressure tube temperature at the top increased slightly and then declined, levelling off at 500°C. This suggested that the pressure tube ballooned into contact with the calandria tube at locations between thermocouple-rings 1 and 2. Temperatures near the top exhibited similar behaviour. Temperatures away from the top of the pressure tube continued to increase until the hottest spot was no longer at the top which was cooled by the contact. During the third period, temperature did not increase significantly despite the increase of power. At the end of this period, the sudden jump in pressure tube temperatures measured at Ring 1 was an indication of a secondary local heat source, probably due to the arcing of failing heaters.

Post test examination of the test section indicates the pressure tube rupture started 60 mm down stream of the garter spring location (mid-plane) and the total rupture length was 620 mm. The calandria tube rupture, unlike the

longitudinal pressure tube rupture, had the form of a hole. The rupture was situated directly above the pressure tube rupture.

SMARTT CODE MODIFICATION AND ASSUMPTION

Two modifications were made to the code for the simulation of the experiments. The internal geometry and material of the fuel-element simulators replaced those of the CANDU fuel. Also, the pressure tube was excluded from the temperature averaging procedure which was used to calculate the steam temperature in each subchannel in the SMARTT model. Thus, the temperature of those subchannels which border the pressure tube was determined solely by the temperature of the fuel elements that border the subchannel. Within the model this provides the highest estimate of the steam temperature so that it will be conservatively overpredicted near the pressure tube.

The following assumptions are used in the simulation of these experiments:

- 1 The steam averaging procedure was used in the steam filled subchannels to determine the coolant temperature. The cooler pressure tube surfaces are ignored in this averaging procedure for the outer subchannel coolant temperature calculations to conservatively overpredict coolant temperatures next to the pressure tube.
- 2 The emissivity of the fuel element simulators and the pressure tube surfaces was assumed to be 0.8 which represents oxidized zirconium. The emissivity of the calandria tube was taken to be 0.33.
- 3 The calandria tube temperature was held constant at the temperature of the liquid in the water tank for each experiment.
- 4 The Urbanic-Heidrick equation [7] is used to calculate the zircaloy-steam reaction rate.
- 5 The flow is assumed to be laminar in the steam filled subchannels and a Nusselt number of 4.0 was used to calculate the sheath-to-coolant heat transfer coefficients. The coolant-to-pressure tube heat transfer coefficients were set equal to sheath-to-coolant heat transfer coefficients in the outer subchannels.
- 6 The channel pressure and the transient power history measured in the experiment were input directly into the SMARTT code.
- 7 The failure criterion used for the pressure tube rupture was 100% local true strain (i.e. failure assumed when

local thickness is reduced to 37% of nominal value).

- 8 The ballooning criterion used for the pressure tube contact with the calandria tube was 16.5% average diametral strain.
- 9 The inferred liquid level determined from both sheath and pressure tube thermocouple measurements was used in these simulations and was directly input to the SMARTT code.
- 10- The SMARTT liquid levels were dropped from one discrete level to the next when the inferred liquid level became approximately halfway between the two discrete levels.

COMPARISON WITH EXPERIMENTAL RESULTS

Power, pressure, and channel liquid-level transients are required as input to SMARTT. The power and pressure transients were obtained directly from the measured values. The liquid level was inferred from plots of the height of the various thermocouples above the bottom of the pressure tube versus the time at which the thermocouple started to indicate temperatures increasing above the saturation temperature of the coolant. This time was interpreted as the time at which the level dropped below the thermocouple position.

Two parameters are chosen to show the comparison between the SMARTT predictions and experimental results, namely, the pressure tube and the heater sheath temperature transients.

EXPERIMENT 1

Figure 8 shows the liquid-level transient which was inferred from the thermocouple measurements (smooth curve) and the step transient used in the simulation. SMARTT predictions are compared against the pressure tube temperature measurements at three axial locations (Rings 1, 2 and 3) and at four circumferential positions (0°, 40°, 80° and 100°) as shown in Figures 9 to 11.

The experimental results show that the top of the pressure tube reached a maximum temperature of about 715°C at Ring 1 at 900 s and the temperature starts to decrease to about 690°C at 1000 s. The maximum temperatures at Rings 2 and 3 were about 680°C at 900s and 715°C s at 1000 s, respectively. This indicates that the pressure tube had partially started to balloon at Ring 1 shortly after 800 s into the transient which is evident by the change in the slope of the temperature profile and the decreasing trend thereafter. The close proximity of the pressure tube to the calandria tube results in an increase of heat transfer by radiation to the

calandria tube. Also the axial increase in heat conduction from Rings 2 and 3 caused the pressure tube temperatures to stabilize or temporarily decrease between 800 s and 900 s.

The agreement between experimental measurements and predictions is good in the early stages of heatup with slight underprediction of the pressure tube temperature at the top of the pressure tube. The underprediction at 100° circumferential position is mainly due to the timing of the liquid-level change scheme used in the SMARTT code. In the later stages of heatup, the pressure tube temperatures are marginally overpredicted at the top. The SMARTT simulation predicted that the pressure tube reached a maximum temperature of 791°C at the top and it failed at the top as the local strain reached the value of 100% which is set as the criteria for pressure tube failure. The simulation predicted that the pressure tube would have ballooned into contact with the calandria tube at 802 s into the transient. The maximum top-to-bottom pressure tube circumferential differential temperatures predicted and measured were 608°C and 537°C, respectively. The pressure tube circumferential temperature profiles at different axial locations at time 800 s are shown in Figure 12. The code overprediction was evident at all three axial locations with the maximum discrepancy at the top of the pressure tube. The overprediction of the pressure tube temperature is the main reason for the early pressure tube failure in the simulation.

The sheath temperature profiles show better agreement with the SMARTT simulation. Figure 13 shows the comparison between the SMARTT simulation and the experimental measurements for TC's 11, 12, 14 and 15 at axial Ring 1. The agreement with TC 11 measurements seems to be less favourable due to the early rise in the SMARTT simulation as a result of the early liquid-level change used in the code. However, the code predictions follow a trend similar to that observed in the experiment.

A heat balance performed on the test section revealed that the input power is 85% of the reported total power (Figure 5) due to electrical losses and measurement errors. The code predictions was based on 100% of the measured transient power which is considered to be the main factor for the overpredictions by the code. In order to asses the effect of heat losses, the SMARTT simulation were repeated for various assumed power losses from 0% to 15%. A comparison of the pressure tube temperatures with SMARTT predictions using different power levels are shown in Figure 14. These results confirm that, with assumed heat loss of 15%, the pressure tube temperatures agree closely with experiment.

EXPERIMENT 2

Figure 15 shows the liquid-level transient which was inferred from the thermocouple measurements. The liquid level in this experiment drops quickly to about 40% full in about 80 s and stabilizes at that level for the rest of the transient. Such level transient is ideal for SMARTT simulation since the difference between the level transition in the experiment and in the discrete method used in the SMARTT code is minimized which results in good agreement between simulation and experiment.

The SMARTT predictions of pressure tube temperatures are compared with the measurements at three axial locations (Rings 1, 2 and 3) and at four circumferential positions (0°, 60°, 80° and 100°) as shown in Figures 16 to 18. Good agreement between predictions and measurements, at the top of the pressure tube, is evident from these figures. However, the pressure tube temperatures were slightly overpredicted at circumferential locations 60° and 80°. The pressure tube ballooned into contact with the calandria tube at Ring 3 at 245 s. The evidence of contact is shown in Figure 18 where the pressure tube temperature at the top starts to decrease at about 245 s. In the experiment, the pressure tube failed at 259 s due to heater failure.

The SMARTT simulations indicate that the pressure tube ruptures at 244.8 s due to local stain. The simulations also indicate that ballooning contact will occur at 245.4 s if local failure is ignored. Based on the excellent agreement of ballooning contact time, the failure criteria is seem to be conservative. The circumferential pressure tube temperature profiles are compared with the SMARTT simulations in Figure 19. Excellent agreement is shown between measurements and predictions at all three axial positions. The predicted circumferential pressure tube temperatures between times 220 s and 246 s encompass the measured temperatures at time 240 s for all three rings. The top-tobottom pressure tube temperature differential seems to be comparable at all three axial locations. The maximum pressure tube differential temperatures measured and predicted were 670°C and 682°C, respectively.

The comparison of heater sheath temperatures for one axial position is shown in Figure 20. The agreement is excellent for TC 14. The code slightly underpredicts the sheath temperature at TC 12, but agreement is better for the maximum temperature at Ring 1 before pressure tube failure. The temperature profile predicted by the code for TC 11 is shifted to the left mainly due to the early drop in liquid level to 42% full at time 55 s while the experimental measurements indicate that TC 11 becomes uncovered at about 100 s into the transient. However, the temperature profiles predicted by the code for TC 11 are very similar to those measured in the experiment.

EXPERIMENT 3

Figure 21 shows the inferred transient liquid level from the thermocouple measurements. The liquid level profile shows an initial fast drop to 76% full at 200 s and slowly decrease to about 55% full by the end of the transient. This type of liquid transient is expected to lead to good agreement between measurement and predictions since the difference between the actual liquid level and the SMARTT discrete liquid level is minimized.

Figures 22 and 23 show the comparison between measurements and predictions for the pressure tube temperature at four circumferential locations (0°, 40°, 60°, 100° for Ring 1 and 0°, 60°, 80°, 100° for Rings 2) at two different axial locations. Reasonable agreement was obtained in the first 300 s at Ring 1 while good agreement was obtained in the same time at Ring 2. The pressure tube temperature was overpredicted from 300 s to the end of simulation (i.e. at Ring 1 (0°, 40°, 60°) and at Ring 2 (0°, 60°)). The predictions at the lower circumferential locations are in an excellent agreement with the measurements. The SMARTT simulation predicted pressure tube failure at 369 s. With the maximum pressure tube temperature at 759°C and the maximum top-to-bottom pressure tube differential temperature at 511°C. It is evident from the pressure tube temperature profiles that the pressure tube ballooned into contact with the calandria tube at about 470 s at Ring 2 where the temperature at the top declined substantially. The thermocouple at the top at Ring 1 failed at that time. The pressure tube was reported to have ruptured at the top at time 1278 s due to heater failure. The maximum measured pressure tube temperature was 720°C at the top before ballooning and the maximum measured top-to-bottom differential temperature was 471°C. Figure 24 shows the comparison between experimental measurements and SMARTT predictions for the pressure tube circumferential temperatures. The agreement is reasonable at lower circumferential locations; however, the temperature is significantly overpredicted at the upper locations of the pressure tube.

The heater sheath temperature profiles both measured and predicted at Ring 3 shown in Figure 25 indicate good agreement. However, the heater sheath temperature at the end of the SMARTT simulation was marginally overpredicted at TC 13.

A heat balance performed on the test section revealed that the input power is 70% of the reported total power (Figure 7) due to electrical losses and measurement errors. The code predictions discussed above was based on 100% of the reported total power which is considered to be the main factor contributing to the overpredictions by the code. A

comparison of the pressure tube temperatures with SMARTT predictions accounting for the heat losses are shown in Figure 26. These results confirm that with assumed heat loss and measurement errors of 30%, the pressure tube temperatures agree closely with experiment.

CONCLUSIONS

- 1 The SMARTT computer code was used to model the Make-Up Water experiments which is part of the pressure tube circumferential differential experimental program. The code was modified to model the heater geometry used in the experiments.
- 2 In general, good agreement was obtained between experimental results and SMARTT predictions. The discrepancies are attributed to the uncertainty in input power measurements and the limited discrete liquid level available in the SMARTT code.
- 3 Modelling efforts are underway to increase the number of discrete liquid levels available in SMARTT to more accurately represent the actual liquid level in experiments. Also, the feedback between geometry changes and thermohydraulic modelling is being considered for implementation in the code.

REFERENCES

- K.E. Locke, G.H. Archinoff, and A.P.Muzumdar, "SMARTT - A Computer Code to Predict Fuel and Pressure Tube Temperature Gradients Under Asymmetric Coolant Conditions", Proc. 6th Annual CNS Conference, Ottawa, June 1985.
- [2] E. Hussein and J.C. Luxat, "Fuel Cooling Under Channel Steam Venting Conditions", Proc. 6th Annual CNS Conference, Ottawa, June 1985.
- [3] G.H. Archinoff, J.C. Luxat, P.D. Low, K.E. Locke, and A.P. Muzumdar, "Simulation Methodology for Pressure Tube Integrity Analysis and Comparison with Experiments", Proc. 2nd International CNS/ANS Conference on Simulation Methods in Nuclear Engineering, Montreal, October 1986.
- [4] K.E. Locke, J.C. Luxat, A.P. Muzumdar, C.B. So, R.G. Moyer, and D.Litke, "Progress on SMARTT Simulation of Pressure Tube Circumferential Temperature Distribution Experiments - Test 1 to 4", Proc. 8th Annual CNS Conference, New Brunswick, June 1987.
- [5] P.S. Yuen, et al, "The Experimental Measurement of Circumferential Temperature Distributions Developed on

- Pressure Tubes Under Stratified Two-Phase Flow Conditions", Proceeding of the 10th Annual CNS Conference, Ottawa, June 1989.
- [6] P.S. Kundurpi, "Validation of the Computer Code for Simulation of Pressure Tube Asymmetric Ballooning Behaviour", Proceeding of the 12th Annual Symposium on Simulation of Reactor Dynamics and Plant Control, Hamilton, April 1986.
- [7] V.F. Urbanic and T.R. Heidrick, "High-Temperature Oxidation of Zircalloy-2 and Zircalloy-4 in Steam", Journal of Nuclear Materials, V.75 (1978), pp. 251-261.

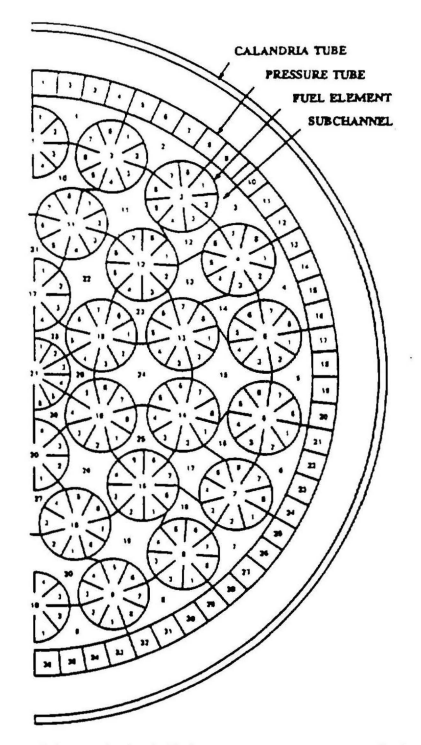


Figure 1: Subchannel, azimuthal fuel-element and pressure-tube nodalization for a 37-element fuel bundle.

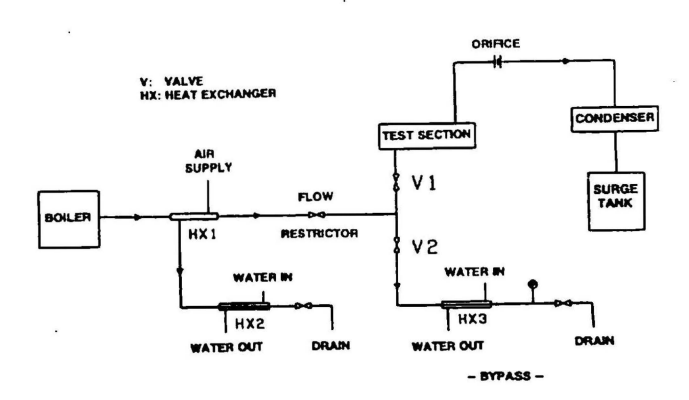


Figure 2: Schematic diagram of experimental apparatus.

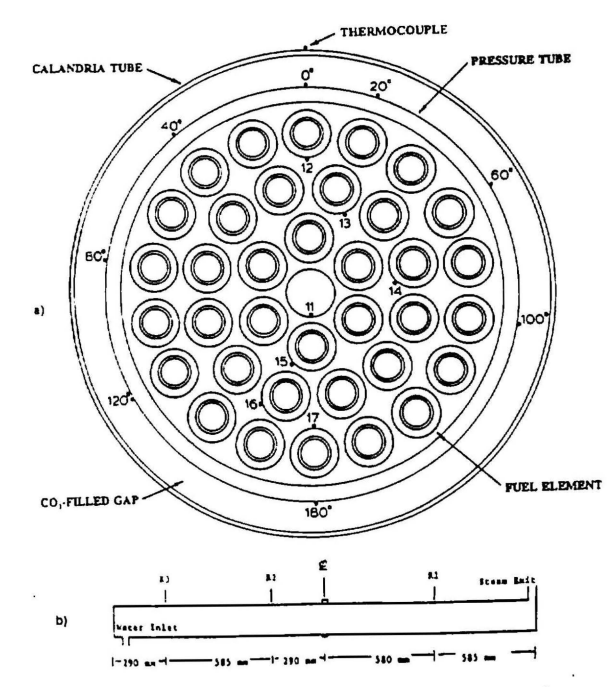


Figure 3: Schemetic diagram of test section, a) cross-sectional view showing the locations of the thermocouples at each axial Ring and b) iongitudinal view showing the locations of the axial Rings.

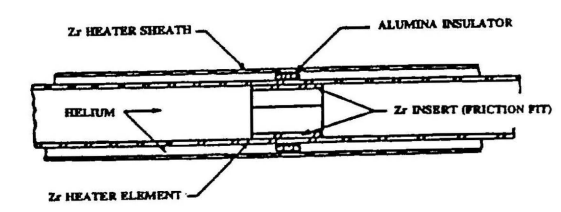


Figure 4: Schematic diagram of the fuel-element simulator.

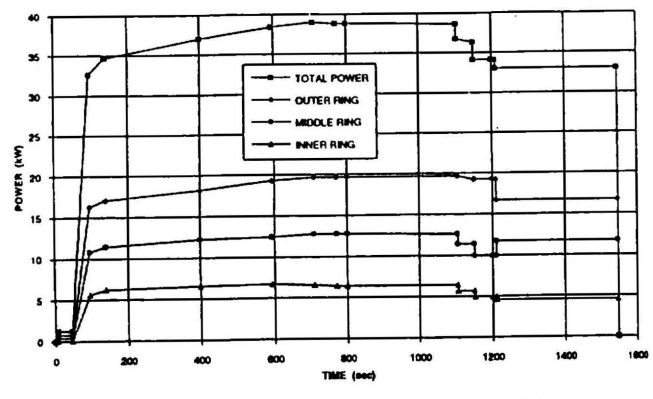


Figure 5: Transient power history for Test 1 of the Make-up Water Series.

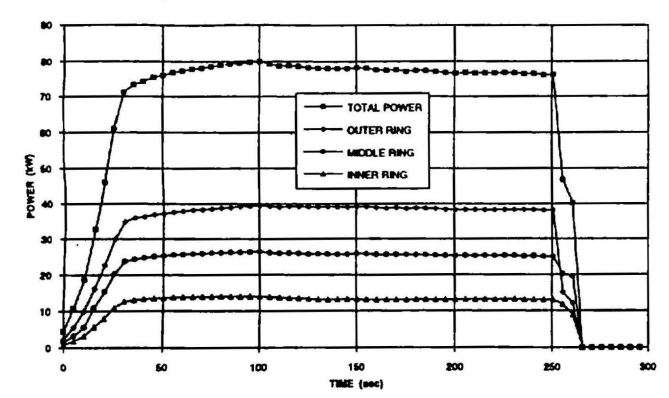


Figure 8: Transient power history for Test 2 of the Make-up Water Series.

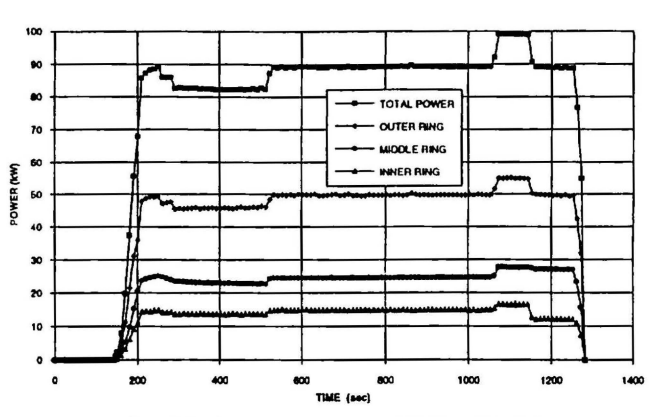


Figure 7: Transient power history for Test 3 of the Make-up Water Series.

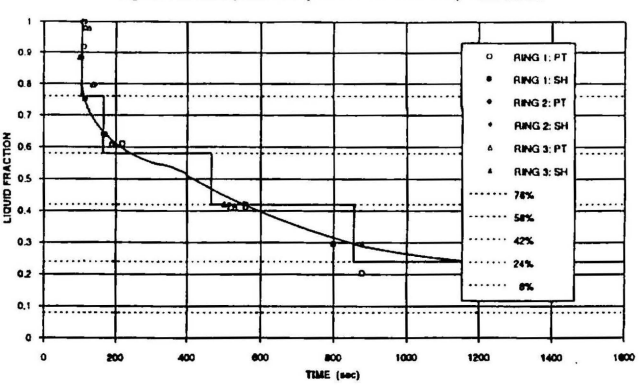


Figure 8: Liquid-level transient for Test 1 of the Make-up Water Series inferred from pressure tube (PT) and sheath (SH) temperature measurements.

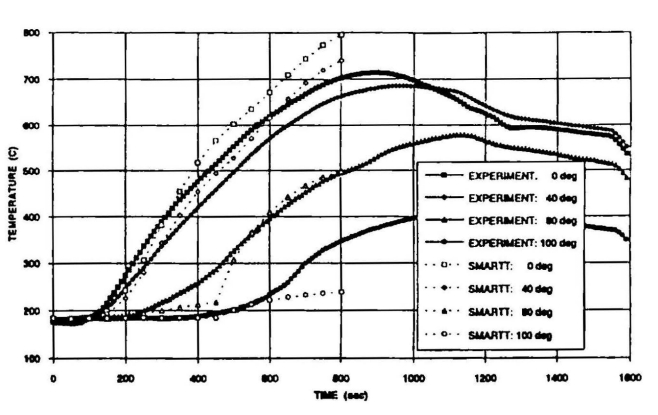


Figure 9: Pressure tube temperatures at Ring 1 for Test 1 of the Make-up Water Series.

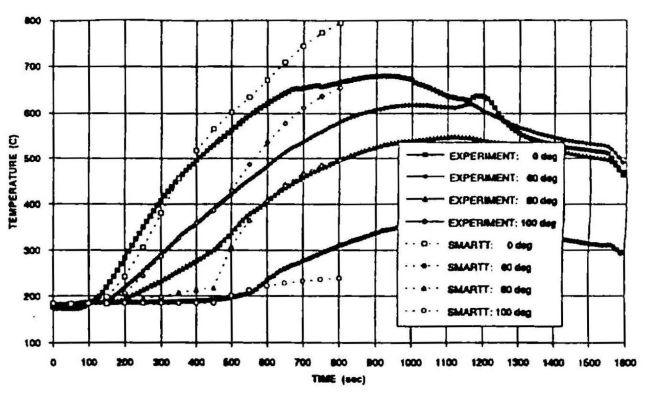


Figure 10: Pressure tube temperatures at Ring 2 for Test 1 of the Make-up Water Series.

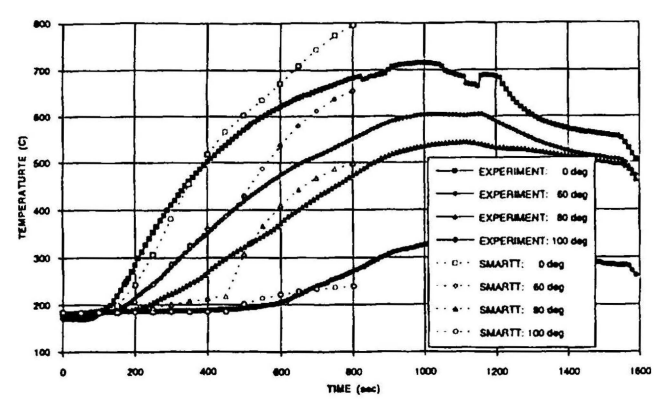


Figure 11: Pressure tube temperatures at Ring 3 for Test 1 of the Make-up Water Series.

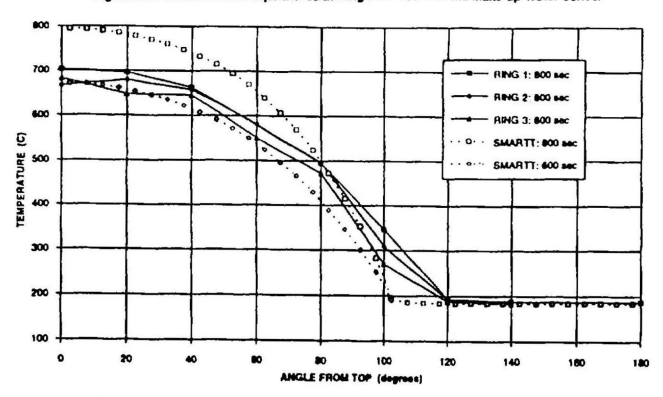


Figure 12: Pressure tube circumferential temperature profiles at three axial locations at time 800 s for Test 1 of the Make-up Water Series.

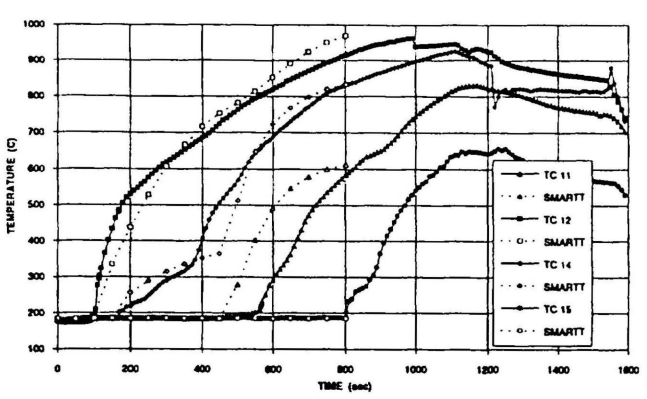


Figure 13: Heater sheeth temperatures at Ring 1 for Test 1 of the Make-up Water Series.

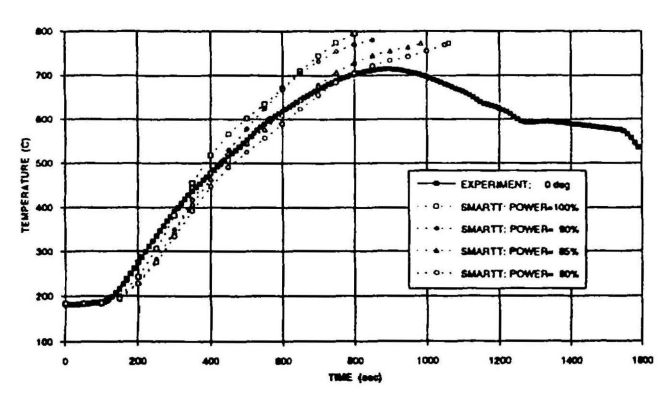


Figure 14: Peak pressure tube temperature at Ring 1 with SMARTT simulations at various fractions of the measured power level for Test 1 of the Make-up Water Series.

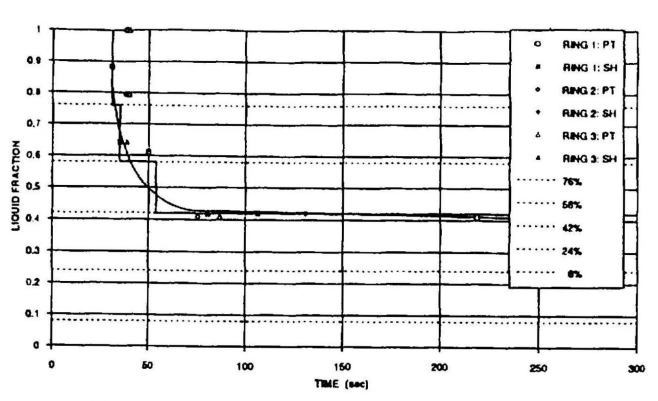


Figure 15: Liquid-level translent for Test 2 of the Make-up Water Series Inferred from pressure tube (PT) and sheath (SH) temperature measurements.

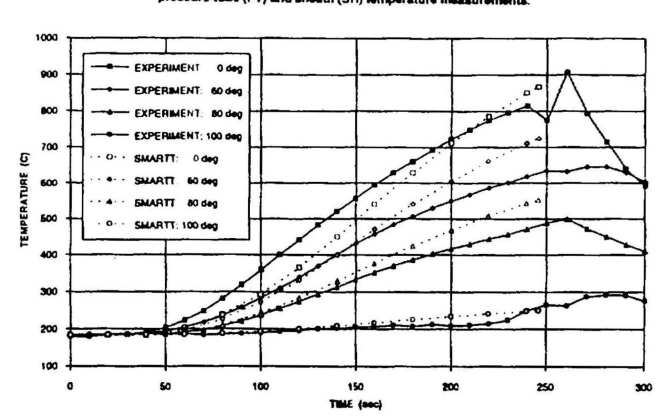


Figure 16: Pressure tube temperatures at Ring 1 for Test 2 of the Make-up Water Series.

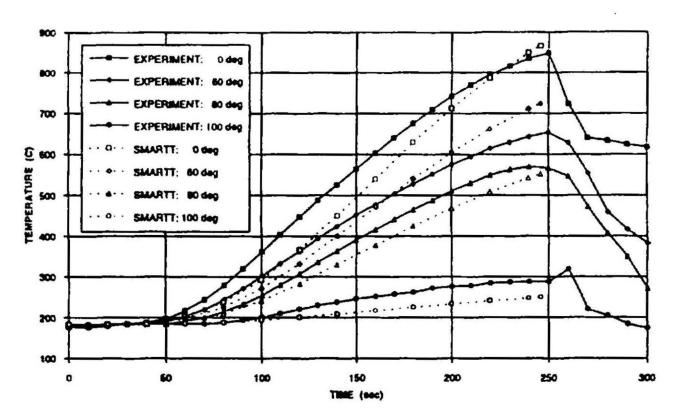


Figure 17: Pressure tube temperatures at Ring 2 for Test 2 of the Make-up Water Series.

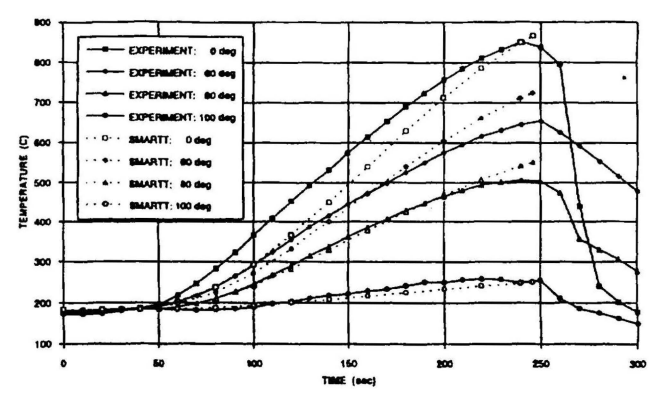


Figure 18: Pressure tube temperatures at Ring 3 for Test 2 of the Make-up Water Series.

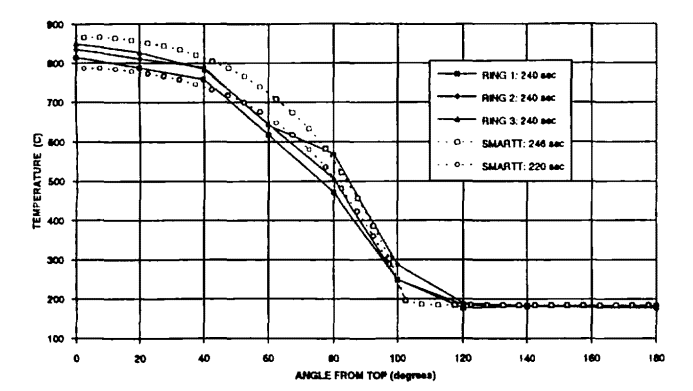


Figure 19: Pressure tube circumferential temperature profiles at three axial locations at time 240 s for Test 2 of the Maks-up Water Series.

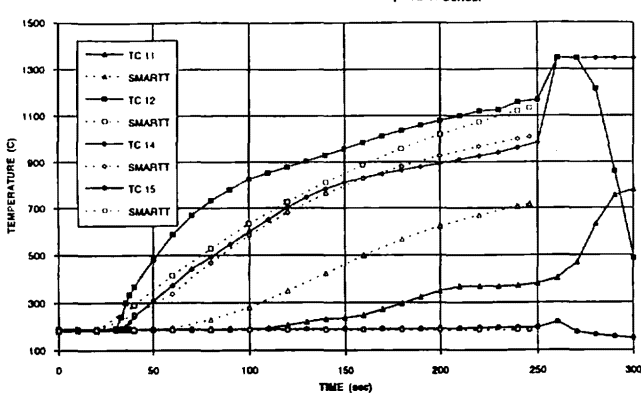


Figure 20: Heater sheeth temperatures at Ring 1 for Test 2 of the Make-up Water Series.

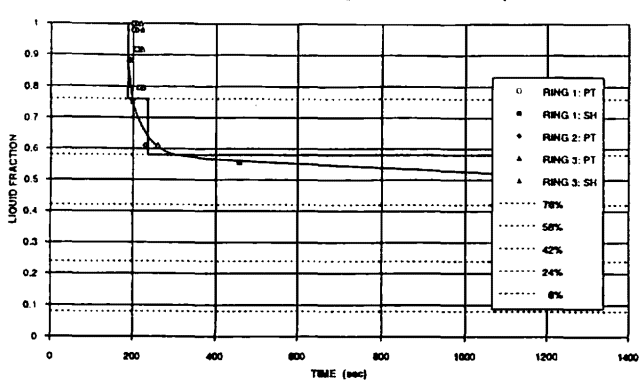


Figure 21: Liquid-level transient for Test 3 of the Make-up Water Series inferred from pressure tube (PT) and sheeth (SH) temperature measurements.

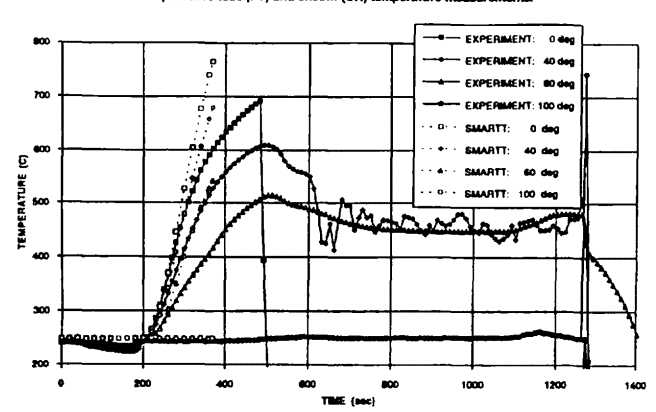


Figure 22: Pressure tube temperatures at Ring 1 for Test 3 of the Make-up Water Series.

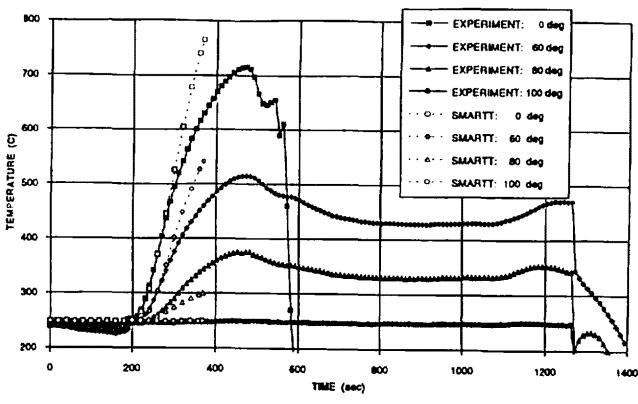


Figure 23: Pressure tube temperatures at Ring 2 for Test 3 of the Make-up Water Series.

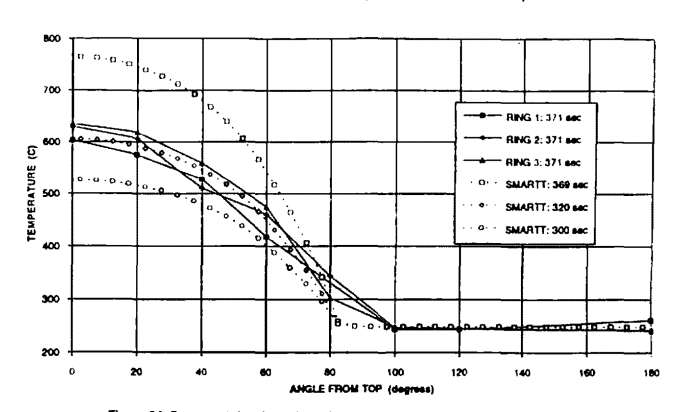


Figure 24: Pressure tube circumferential temperature profiles at three axial locations at 371 s for Test 3 of the Make-up Water Series.

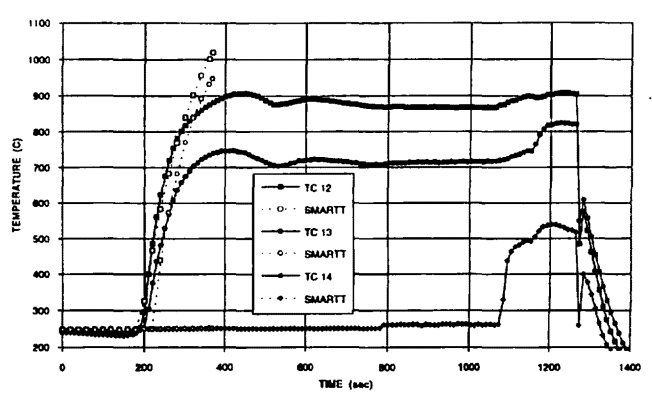


Figure 25: Heater sheath temperatures at Ring 3 for Test 3 of the Make-up Water Series.

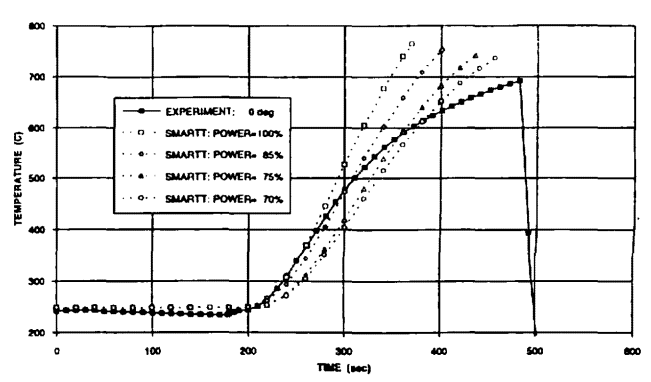


Figure 26: Peak pressure tube temperature at Ring 1 with SMARTT simulations at various fractions of the measured power level for Test 3 of the Make-up Water Series.